Subharmonics and Chaos in Switched Reluctance Motor Drives

K.T. Chau, J.H. Chen, C.C. Chan, and Q. Jiang
Department of Electrical and Electronic Engineering, The University of Hong Kong, Pokfulam, Hong Kong

Abstract – In this paper, the investigation of the nonlinear dynamics of an adjustable speed switched reluctance motor (SRM) drive with voltage PWM regulation is carried out. The corresponding bifurcation diagrams and chaotic Poincaré sections are presented. It shows that the system generally exhibits a period-doubling route to chaos.

I. INTRODUCTION

Subharmonics and chaos in switched mode power supplies have been actively investigated for a number of years [1], [2]. Chaos in induction and brushless dc motor drives have recently been discussed [3], [4]. Very recently, subharmonics and chaos in industrial dc motor drives have also been analyzed [5], [6]. It is the purpose of this paper to investigate the nonlinear dynamics (including subharmonics and chaotic behaviors) of SRM drives using voltage PWM regulation. Firstly, nonlinear iterative mappings based on nonlinear and approximately linear flux linkage models are derived. Then, the corresponding computer simulation is carried out to study the subharmonics and chaotic behaviors.

II. MODELING OF SRM DRIVE SYSTEMS

As shown in Fig. 1, an adjustable speed SRM drive system is used for exemplification, where speed control is achieved through PWM control of motor phase voltage. The ramp voltage v_r is a function of the instantaneous rotor displacement $\theta(t)$:

$$v_r(\theta(t)) = v_l + (v_u - v_l)\theta(t)/\theta_T \tag{1}$$

where v_l and v_u are the lower and upper bounds of the ramp voltage, $\theta_T = (\theta_c - \theta_o)/n_\theta$ its period, θ_o and θ_c are turn-on and turn-off angles, and n_θ an integer. As the op-amplifier OA has a feedback gain g, the speed control signal $v_c(t)$ is:

$$v_c(t) = g(\omega(t) - \omega_{ref}) \tag{2}$$

where $\omega(t)$ and ω_{ref} are the instantaneous and reference speeds. Ignoring the mutual inductances with other phase windings, the system equation based on the nonlinear flux linkage model is given by:

$$\begin{cases} \dfrac{d\theta}{dt} = \omega \\ \dfrac{d\omega}{dt} = \left(\dfrac{\partial W'_m(\theta, i_1, \cdots, i_m)}{\partial \theta} - B\omega - T_L\right)/J \\ \dfrac{di_k}{dt} = \left[\dfrac{\partial \psi_k}{\partial i_k}(\theta, i_k)\right]^{-1}\left[u_k - Ri_k - \omega \dfrac{\partial \psi_k}{\partial \theta}(\theta, i_k)\right] \ (k = 1, \cdots, m) \end{cases} \tag{3}$$

where u_k, i_k, $\psi_k(\theta, i_k)$ are the kth phase voltage, current, and flux linkage, respectively, $W'_m(\theta, i_1, \cdots, i_m)$ co-energy of all m phases, R phase resistance, L phase inductance, B viscous damping, J load inertia, T_l load torque.

Due to the switching operation, the system given by (3) is in fact a time-varying nonlinear state equation. Thus, this drive system is a higher-order non-autonomous dynamic system. Let $\mathbf{X} = (\theta, \omega, i_1, \cdots, i_m)$, (3) can be rewritten as:

$$\dot{\mathbf{X}} = f(\mathbf{X}, t) \qquad \mathbf{X}(t_0) = \mathbf{X}_0 \tag{4}$$

Then, its solution in continuous-time domain is given by:

$$\phi_t(\mathbf{X}_0, t_0) = (\theta(\mathbf{X}_0, t_0), \omega(\mathbf{X}_0, t_0), i_1(\mathbf{X}_0, t_0), \cdots, i_m(\mathbf{X}_0, t_0))_t \tag{5}$$

III. DERIVATION OF POINCARÉ MAP

Focusing on the investigation on subharmonics and chaotic behaviors in drive systems, the most attractive approach has been the iterative nonlinear mapping so-called Poincaré map [2], [7]. Since SRM phase windings are alternatively conducted, the dc-link current $i_{dc} = i_1 + \cdots + i_m$ is selected as a new state variable. The new state vector is:

$$\begin{aligned} \mathbf{Y} &= (\theta, \omega, i_{dc}) \\ &= (\theta(\mathbf{X}_0, t_0), \omega(\mathbf{X}_0, t_0), i_1(\mathbf{X}_0, t_0) + \cdots + i_m(\mathbf{X}_0, t_0))_t \end{aligned} \tag{6}$$

which will be used to describe the dynamics of the drive system. A plane is defined as:

$$\Sigma := \{\mathbf{Y} : (\theta \bmod \theta_T) = 0\} \tag{7}$$

The trajectory of $\mathbf{Y}$ under observation repeatedly passes through Σ when θ increases monotonically. The sequence of Σ crossing defines a map:

$$P : \Re^2 \to \Re^2 \quad (\omega, i_{dc})_{n+1} = P((\omega, i_{dc})_n) \tag{8}$$

The Poincaré map (8) is a two-dimensional mapping, but it is based on the solution (5) of the (m+2)-dimensional non-autonomous equation (4). For the sake of simplicity, when the drive system operates in a lighter load and lower speed condition an approximately linear flux linkage model can be represented as $L(\theta)i$ where:

$$L(\theta) = \begin{cases} L_{min} & 0 < \theta_1 \le \theta \\ L_{min} + K_l\theta & \theta_1 < \theta \le \theta_2 \\ L_{max} & \theta_2 < \theta \le \pi/N_r \end{cases} \tag{9}$$

The intervals of $(0, \theta_1)$ and $(\theta_2, \pi/N_r)$ are the unaligned and the aligned overlap section, respectively. N_r is the number of the SRM rotor. For each phase winding, selecting that $\theta_o = \theta_1$, $\theta_c = \theta_2$, and $\theta_c - \theta_o$ equals to the phase-shift angle θ_s, the electromagnetic torque in the conduction interval

$\theta_c - \theta_o$ always is $K_l i_k^2/2$. Assuming that i_k gradually becomes zero in period of L_{max}, there is no electromagnetic torque produced by this phase winding in this period. Thus, i_k in this period can be ignored since the initial value of the successive phase current must be zero. Therefore, (4) can be deduced as:

$$\begin{cases} \dfrac{d\theta}{dt} = \omega \\ \dfrac{d\omega}{dt} = (\dfrac{1}{2} K_l i^2 - B\omega - T_L)/J \\ \dfrac{di}{dt} = \dfrac{u - Ri - K_l \omega i}{L_{min} + K_l \theta} \end{cases} \quad (10)$$

The Poincaré map based on the solution of (10) becomes:

$$(\omega, i)_{n+1} = P((\omega, i)_n) \quad (11)$$

It is important to note that this map, based on the approximately linear flux linkage model, facilitates the investigation of the nonlinear dynamics mainly caused by the switching nonlinearity. Since (10) can be expressed as an analytical formula, it not only takes less computational time, but also enables the qualitative analysis of nonlinear characteristics.

IV. Computer Simulation

To illustrate the derived modeling, computer simulation is carried out. Practical component and parameter values of the SRM drive system are selected: m = 3, N_s = 12, N_r = 8, θ_1 = 5.5°, θ_2 = 20.5° θ_s = 15°, R = 0.1 Ω, L_{min} = 0.34 mH, K_l = 7.8 mH/rad, B = 0.0005 Nm/rads^{-1}, J = 0.025 Nm/rads^{-2}, T_l = 1 Nm; v_u = 4 V v_l = 0 V, θ_T = 7.5°, g = 10 V/rads^{-1}, U = 100 V, ω_{ref} = 100 rad/s.

By employing standard numerical techniques [7] to compute the Poincaré map (11) based on the approximately linear flux linkage model of SRM drive systems, the bifurcation diagrams and chaotic waveforms and Poincaré section can be obtained. Since that $\theta_T = (\theta_c - \theta_o)/2$, the stable steady solution will be period-2 whose frequency for ω_{ref} = 100 rad/s is about 382 Hz. The period-2 waveforms of v_c and v_r for g = 10 V/rads^{-1} are shown in Fig. 2. The chaotic waveforms of v_c and v_r for g = 20 V/rads^{-1} and the corresponding Poincaré section are shown in Figs. 3 and 4. It indicates that there is cycle skipping when the system operates in chaos. The bifurcation diagrams of the speed ω and current i versus gain g from 10 to 20 V/rads^{-1} are shown in Figs. 5 and 6, respectively. It can be found that there are coexisting attractors between 15.5 and 17.5 V/rads^{-1}. Changing ω_{ref} to 50 rad/s, the bifurcation diagrams of ω and i versus g from 2 to 6 V/rads^{-1} are shown in Figs. 7 and 8, respectively. All of bifurcation diagrams show that the system exhibits a typical period-doubling route to chaos. Comparing Figs. 7 and 8 with Figs. 5 and 6, it can be found that the structure of bifurcation diagrams depends highly on the choice of the parameters that remain fixed. The value of bifurcation parameter g bifurcating to chaotic behavior for ω_{ref} =50 rad/s is much less than one for ω_{ref} =100 rad/s. It seems that higher g and lower ω is prone to subharmonics and chaos. When the drive system operates in the subharmonics and chaos, the oscillating magnitude of the phase current rapidly increases from about 30 A to 40 A and even more. This is one of key reasons that the chaos should be avoided.

V. Conclusion

In this paper, the Poincaré map of the SRM drive system with voltage PWM regulation has been derived. Based on the derived map, the characteristics of subharmonics and chaotic behaviors have been investigated by computer simulation. It reveals that the system exhibits a typical period-doubling route to chaos. The Poincaré map can greatly facilitate the identification of the desired stable operating ranges during different system parameters and conditions.

Although the investigation has been focused on a typical SRM drive, the proposed approach and derived equations can readily be applied or extended to other SRM drives.

VI. Acknowledgment

This work was supported and funded in part by the CRCG of the University of Hong Kong, and the Hong Kong Research Grants Council.

VII. References

[1] J.R. Wood, "Chaos: a real phenomenon in power electronics," IEEE APEC Proc., 1989, pp.115-123.

[2] D.C. Hamill, J.H.B. Deane, and D.J. Jefferies, "Modeling of chaotic dc-dc converters by iterated nonlinear mappings," IEEE Trans. Power Electronics, Vol. 7, 1992, pp. 25-36.

[3] I. Nagy, L. Matakas, Jr., and E. Masada, "Application of the theory of chaos in PWM technique of induction motors," IPEC Proc., 1995, pp. 58-63.

[4] N. Hemati, "Strange attractors in brushless DC motors," IEEE Trans. Cir. System-I, Vol. 41 , 1994, pp. 40-45.

[5] K.T. Chau, J.H. Chen, C.C. Chan, Jenny K.H. Pong, and D.T.W. Chan, "Chaotic behavior in a simple dc drive," IEEE PEDS Proc., Vol. 1, 1997, pp. 473-479.

[6] K.T. Chau, J.H. Chen, and C.C. Chan, "Dynamic bifurcation in dc drives," IEEE PESC Proc., 1997, pp. 1330-1336.

[7] T.S. Parker and L.O. Chua, *Practical Numerical Algorithm for Chaotic Systems*, New York; Springer-Verlag, 1989.

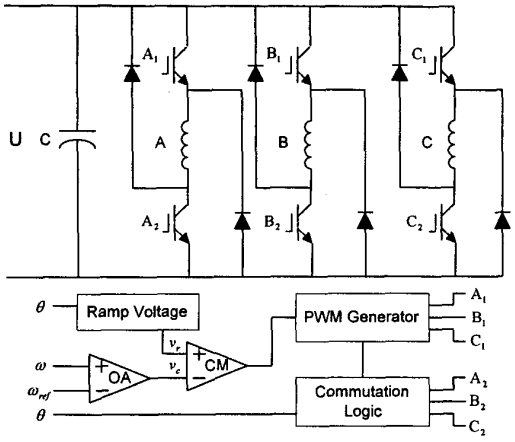

Fig. 1 Schematic diagram of SRM drive system.

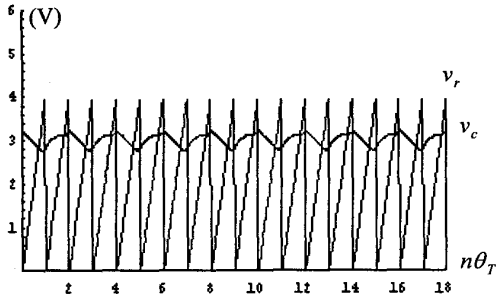

Fig. 2 Period-2 waveforms of v_c and v_r.

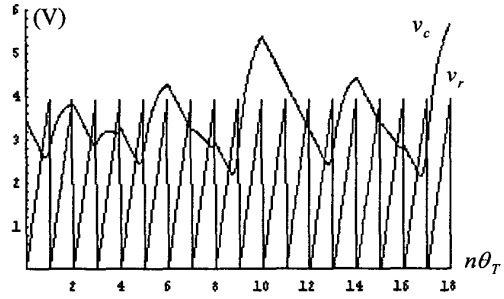

Fig. 3 Chaotic waveforms of v_c and v_r.

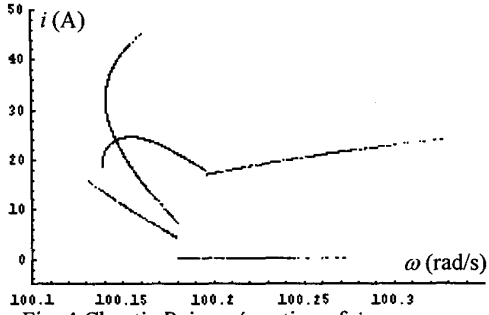

Fig. 4 Chaotic Poincaré section of i versus ω.

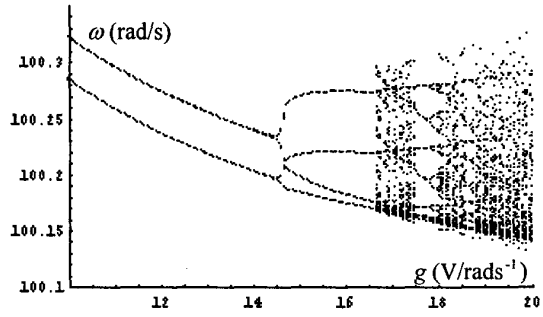

Fig.5 Bifurcation diagram of ω versus g for ω_{ref} =100rad/s.

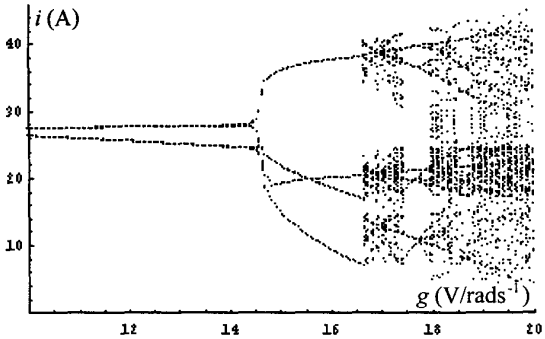

Fig. 6 Bifurcation diagram of i versus g for ω_{ref} =100rad/s.

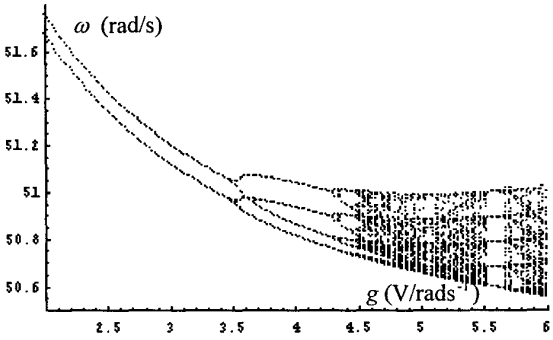

Fig.7 Bifurcation diagram of ω versus g for ω_{ref} =50rad/s.

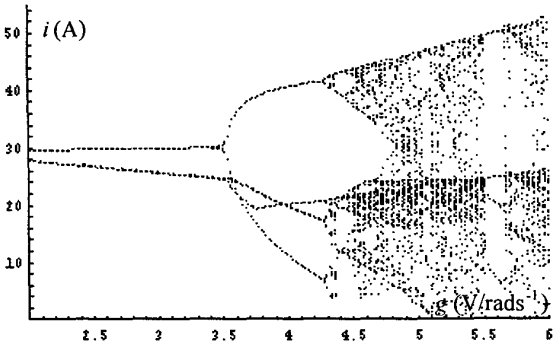

Fig. 8 Bifurcation diagram of i versus g for ω_{ref} =50rad/s.